



**HAL**  
open science

## Displacement Damage Effects in InGaAs Photodiodes due to Electron, Proton, and Neutron Irradiations

Thierry Nuns, Christophe Inguibert, Juan Barbero, Juan Moreno, Samuel  
Ducret, Alexandru Nedelcu, Bjorn Galnander, Elke Passoth

► **To cite this version:**

Thierry Nuns, Christophe Inguibert, Juan Barbero, Juan Moreno, Samuel Ducret, et al.. Displacement Damage Effects in InGaAs Photodiodes due to Electron, Proton, and Neutron Irradiations. IEEE Transactions on Nuclear Science, 2020, 67 (7), pp.1263-1272. 10.1109/TNS.2020.2984133 . hal-03075355

**HAL Id: hal-03075355**

**<https://hal.science/hal-03075355>**

Submitted on 16 Dec 2020

**HAL** is a multi-disciplinary open access archive for the deposit and dissemination of scientific research documents, whether they are published or not. The documents may come from teaching and research institutions in France or abroad, or from public or private research centers.

L'archive ouverte pluridisciplinaire **HAL**, est destinée au dépôt et à la diffusion de documents scientifiques de niveau recherche, publiés ou non, émanant des établissements d'enseignement et de recherche français ou étrangers, des laboratoires publics ou privés.

# Displacement damage effects in InGaAs photodiodes produced by electrons, protons and neutrons irradiations

T. Nuns<sup>1</sup>, C. Inguibert<sup>1</sup>, J.Barbero<sup>2</sup>, J. Moreno<sup>2</sup>, S. Ducret<sup>3</sup>, A. Nedelcu<sup>3</sup>, B. Galnander<sup>4</sup>, E. Passoth<sup>4</sup>

**Abstract**— A large set of InGaAs photodiodes from different manufacturers has been irradiated with electrons from 0.5 MeV up to 20 MeV, with protons of 60 MeV, 100 MeV and 170 MeV and with atmospheric-like neutrons spectrum. Depending on the type of incident particles and energy, deposited damage dose have been evaluated in the  $\sim 5 \times 10^6$  -  $5 \times 10^9$  MeV/g range. The dark current damage factor has been extracted from measurements at different fluence levels. Dark current data right after irradiation and two months later allows for evaluating any possible annealing processes. The damage factor measured after about two months has been scaled with Non Ionizing Energy Loss (NIEL). Finally, validity of NIEL scaling is discussed for InGaAs materials.

**Index Terms**— Space Environment, Displacement Damage, gamma rays, Non Ionizing Energy Loss.

## I. INTRODUCTION

Energetic particles, when they travel through matter, interact with atomic nuclei and provoke displacements and defects in monocrystalline lattices. Fluxes of particles encountered in space are large enough to produce sufficient amount of defects and significantly degrade semiconductor materials. Produced electrically active defects act as generation/recombination centres affecting the functioning of electronic devices. Optoelectronic components are particularly sensitive to such phenomenon. Some degradation, like increase of dark current, are proportional to the amount of defects. In this case, degradation is thus proportional to the incident fluence. However, the capability of incident particles to produce defects varies depending on particle species, and for a given particle type, on energy. The damage coefficient is defined as dark current increase to incident fluence ratio. Hence, the damage coefficient differs from one type of radiation to another. It also depends on the incident energy. Therefore, fluence is not the best metric to scale the degradation induced by displacement damage effects. Indeed,

the number of produced defects is proportional to the non-ionising dissipated energy. The incident particles interact with nuclei of the target material thanks to nuclear interactions (Coulombian, nuclear elastic and inelastic). According to binary collision approximation, the number of displaced atoms is equal to the dissipated energy divided by twice the minimum energy required to displace an atom ( $T_d$ ). To the first order, the final number of defects is shown to be proportional to the number of atomic displacements and thus to energy dissipated in terms of nuclear interactions, i.e. Displacement Damage Dose (DDD). The displacement damage dose deposited per incident particle is given by Non Ionizing Energy Loss (NIEL) [1]-[5], which is shown to be the best parameter to scale degradations induced in microelectronic devices by atomic displacements. The well-known “NIEL scaling approach”, that consists in considering that damage factor is proportional to NIEL, is shown to work quite well in most of cases [6]-[9]. Apart from some deviations observed for electrons [10]-[21] in both Si and GaAs, high energy protons in GaAs [22]-[24] and neutrons in GaAs [25], the NIEL scaling approach is proven to be effective for silicon and gallium arsenide material, for which it is widely used [6]-[9].

It is with electrons that deviation from NIEL scaling is most frequently observed, whatever the semiconductor Si [7][16][17][20] and GaAs [10]-[15][18][19][21].

Furthermore, space applications in infrared domain have been growing rapidly, requiring good knowledge of resistance to radiation of semiconductor materials such as II-VI (HgCdTe), or III-V (InGaAs). Compared to Si and GaAs, InGaAs material has not been extensively studied. Extracting general rules requires large set of data obtained with various particle species and energies [26].

Useful data in the literature comes from devices having different technological characteristics that can affect measured damage factor. Moreover, damage factors associated to different electrical parameters (dark current, diffusion length) can be mixed and the response to radiation varies from one parameter to another. For example, in solar cells degradation, short circuit current evolution differs from power loss. In addition, test conditions are often not identical. For instance, temperature and annealing time impact directly measurements.

The aim of this work is to measure the dark current degradation of photodiodes from a single set of devices

(1) C. Inguibert, T. Nuns are with ONERA, 2 av. E. Belin, 31055 Toulouse, France (e-mail: christophe.inguibert@onera.fr tel: +33-562252734).

(2) J. Barbero, J. Moreno are with ATN ALTER TECHNOLOGY TÜV NORD S.A.U., C/ Majada 3, 28760 Tres Cantos – Madrid, Spain. (e-mail: [juan.barbero@altertechnology.com](mailto:juan.barbero@altertechnology.com) tel: +34-918041893).

(3) S. Ducret, A. Nedelcu are with LYNRED, 364, route de Valence - Actipole - CS 10021 38113. Veurey-Voroize, France.

(4) B. Galnander, E. Passoth are with TSL hunbergsvägen 5A, 751 21 Uppsala, Sweden.

(batch), irradiated and tested with identical conditions. A large set of irradiation conditions is applied on this set of devices. It is then possible to analyse validity of NIEL scaling approach for InGaAs material, based on a large set of irradiation data. The detailed structure of each photodiode is not known (confidential data from manufacturer). Therefore only a relative comparison between these different devices is proposed. We should also remark that dark current increase is not the only degradation that may occur on such devices. Indeed, quantum efficiency may be affected. This parameter is related to the carriers' lifetime and recombination processes in regions where their concentration is in excess, whereas our study focused on dark current in depleted regions.

Three device types coming from different manufacturers (Excelitas, OSI, and LYNRED) have been tested with electrons of energies 0.5, 1.5, 6, 12, and 20 MeV. They have also been irradiated with protons of 60, 100 and 170 MeV, and with atmospheric-like neutron spectrum (equivalent damage energy of  $\sim 2$  MeV). Damage factor has been extracted and compared to NIEL calculated with NEMO [4] package of ONERA implemented in OMERE [38] toolkit.

Section II briefly describes the method for calculating NIEL with a focus on neutrons case. Section III presents the experimental setup, describing devices, irradiation facilities, test and irradiation conditions. Section IV presents dark current increase and section V compares dark current damage factor with NIEL.

## II. NIEL CALCULATION

NIEL, which is average energy loss imparted in atomic displacement, is classically given by [4]:

$$NIEL = \eta \cdot \int_{T_d}^{Q_{max}} \frac{d\sigma}{dQ} \cdot G(Q) \cdot Q \cdot dQ \quad (1)$$

Where  $\eta$  is the atomic density of target material,  $T_d$  threshold displacement energy and  $Q_{max}$  maximum energy level that the incident particles can yield to target's nuclei.  $d\sigma/dQ$  is the differential interaction cross section per unit of transferred energy, thus  $Q$  is the recoil energy imparted to target atoms.  $G(Q)$  is the energy partition function that provides part of recoil energy that goes into atomic displacements. The energy partition function of Lindhard [30] is used in our calculation [4], with threshold displacement energies of 10 eV, 10 eV and 15 eV for respectively Ga, As and In. Other key parameters of the calculation are interaction cross sections  $d\sigma/dQ$ . For protons, elastic interaction cross sections (Coulombian + nuclear elastic) have been estimated following the partial wave method [4]. For electrons the Mc Kinley & Fesbasch-screened coulomb cross section expression is employed [31]. For nuclear reactions induced by protons and neutrons, GEANT4 10.patch02 library has been used [32].

In case of protons and neutrons, but more generally for hadrons above some tens of MeV, nuclear reactions take place quite abundantly and must be taken into account in NIEL calculations. For protons and ions below  $\sim 10$  MeV, these nuclear reactions can be ignored. Indeed, the Coulombic potential barrier prevents protons from inducing such reactions. This is not the case for neutrons that are able to

produce nuclear reactions even at very lower energy levels. The neutron NIEL has been calculated with GEANT4 using FTFP\_BERT\_HP physic option [32]. This option is based on the Bertini Cascade model valid in range  $[\sim \text{MeV}, 15 \text{ GeV}]$  thanks to the use of a pre-compound model below  $\sim 100$  MeV [33]. The High Precision (HP) option allows an accurate simulation of nuclear reactions (elastic + inelastic) thanks to the use of G4NDL nuclear reaction database. To summarize, in the energy range of interest  $[\sim 100 \text{ keV}, \sim 1 \text{ GeV}]$  FTFP\_BERT\_HP physical option of GEANT4 uses the reference Bertini cascade model above 75 MeV and switch to the pre-equilibrium and nuclear evaporation models native to the Bertini code down to 20 MeV. Below 75 MeV, the former offers better precision than intra-nuclear cascade model better suited for higher energies. G4NDL database is used thanks to the HP option below 20 MeV. G4NDL data comes from different releases of evaluated data libraries (e.g. ENDF/B-VII.1, JEFF-3.3, JENDL-4.0, etc.), which have been converted into Geant4 format [32]. HP database (ENDF files) reconstructs the resonance cross section observed at low energy according to procedure similar to NJOY [34] for both elastic and inelastic reactions [32]. Validations of those models can be found in [35].

NIEL calculations have been validated by comparison with neutron NIEL from SR-NIEL code [36] and ASTM standard [37]. As can be seen in Fig. 1, agreement is very good for silicon material.

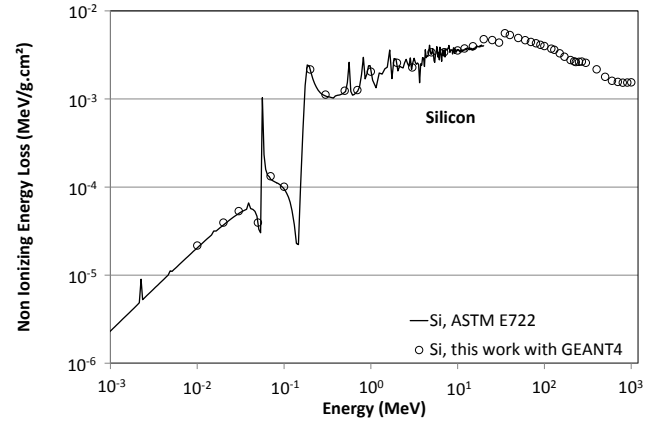


Fig. 1: NIEL of neutrons in silicon. Comparisons of our GEANT4 calculation with ASTM KERMA [37].

For compound materials  $A_xB_y$  comprising two elements A and B with respective stoichiometry  $x$  and  $y$ , NIEL is simply the weighted sum of NIELs of single elements constituting the material:

$$NIEL_{A_xB_y} = x \frac{M_A}{M_{A_xB_y}} NIEL_A + y \frac{M_B}{M_{A_xB_y}} NIEL_B \quad (2)$$

Where  $M_A$ ,  $M_B$  and  $M_{A_xB_y}$  are respectively the molar mass of elements A, B. Calculations have been performed for GaAs and InGaAs materials. For GaAs, similarly to silicon material, comparison has been performed with SR-NIEL code [36] and ASTM standard [37] data. The agreement with KERMA of both references is quite good (cf. Fig. 2). A maximum difference of  $\sim 30\%$  is observed with our calculations. This is

not surprising since the different calculations employed different nuclear reaction databases.

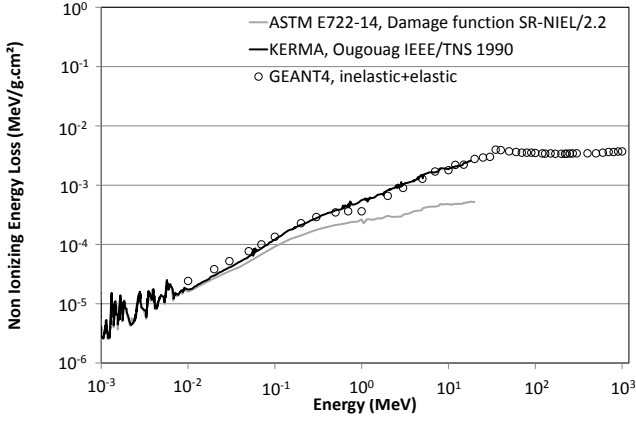


Fig. 2: NIEL of neutrons in GaAs. Comparison of our GEANT4 calculations with ASTM KERMA [25], [37] and with damage function of ASTM E722-14 calculated with SR-NIEL code [36]. In order to compare different functions in absolute terms, the damage function is presented in the figure divided by normalization factor 2.2 used in ASTM.

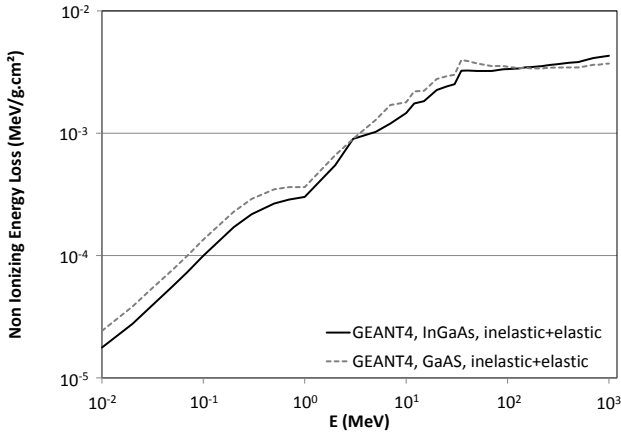


Fig. 3: Comparison of NIEL of neutrons in GaAs and InGaAs. Calculations are performed with our GEANT method.

Calculations have been next extended to InGaAs material (Fig. 3) for a chemical composition  $\text{In}_x\text{Ga}_{1-x}\text{As}$  with  $x = 0.53$ . As can be seen in Fig. 3, NIEL of GaAs and InGaAs are very close to each other.

InGaAs NIEL was compared with experimental data (cf. section V). Some devices have been irradiated with atmospheric like ANITA neutron spectrum of the TSL facility. This spectrum is presented in section III. For comparison with experimental measured damage factors, the equivalent damage energy  $E_q$  with ANITA spectrum has been calculated according to the following formula:

$$\frac{\int_{E_{\min}}^{E_{\max}} \frac{d\Phi}{dE}(E) \cdot \text{NIEL}_{n,\text{InGaAs}}(E) \cdot dE}{\int_{E_{\min}}^{E_{\max}} \frac{d\Phi}{dE}(E) \cdot \text{NIEL}_{n,\text{InGaAs}}(E_q) \cdot dE} = \text{NIEL}_{n,\text{InGaAs}}(E_q) \quad (3)$$

The equivalent energy of ANITA spectrum has been estimated to  $E_q \approx 2$  MeV and used to scale measured induced damage factors in InGaAs.

### III. EXPERIMENTAL SETUP

#### A. Tested photodiodes

Photodiodes tested in this study come from three different manufacturers: Lynred, Excelitas and OSI.

Lynred [39] provided test vehicles manufactured in the same technology as SNAKE device. This device is a new generation of VGA (Video Graphics Array) InGaAs FPA (Focal Plane Array) sensor with high level of sensitivity and resolution dedicated to low flux applications. It operates in the 0.9  $\mu\text{m}$  to 1.7  $\mu\text{m}$  wavelength domain. Each test vehicle includes a set of InGaAs PIN photodiodes having different topologies. Some of them are circular single photodiodes with different dimensions (diameter in the range [4  $\mu\text{m}$ , 300  $\mu\text{m}$ ]). Some of them are 10x10 sub-arrays of pixels with various pitches (in the range [10  $\mu\text{m}$ , 30  $\mu\text{m}$ ]). Whereas circular photodiodes are addressed separately, all pixels of sub-array are addressed in parallel (all together) so that the measured current is the sum of the contribution of all photodiodes in the sub-array. We limited our measurements to six photodiodes or sub-arrays per test vehicles, selected within the available topologies. We did not have enough identical test vehicles in order to cover all irradiation conditions. Some slight differences occur from one sample to another, in terms of photodiode topology. As a consequence, measured photodiodes may not be exactly the same for each irradiation. Anyway, these differences allow us to focus on damage factor and influence of the photodiode sizes on degradation. All measurements presented here are performed at -5 V.

The second tested device is PIN photodiode C30618 from Excelitas [40]. This high speed single InGaAs circular photodiode is designed for use in OEM fiber-optics communications systems and high-speed receiver applications. It operates between 1000 nm and 1600 nm and has a diameter of 350  $\mu\text{m}$  and maximum intrinsic dark current of typical  $\sim 1$  nA with an applied voltage of -10V (bias at which current measurements were made).

The last tested device is FCIQ1000 from OSI Optoelectronics [41]. FCI-InGaAs-QXXX series are large active circular area InGaAs photodiodes segmented into four quadrants. As a consequence, each device has four photodiodes, all measured independently in our study. The Q1000 device active diameter is 1000  $\mu\text{m}$  and presents a 0.5 nA dark current at -5V (bias for the current measurements). The Q1000 photodiode is optimized for good responsivity from 1100 nm to 1620 nm.

The two latter devices have been selected because of their relatively large active areas with several hundreds of micrometers of diameter, and present relatively low intrinsic dark currents. The goal was to have optimal conditions in order to get the greatest sensitivity to radiation. Because all OSI or Excelitas irradiated samples are identical whatever irradiation conditions (in the contrary of SNAKE test vehicles), obtained data are used for direct comparison of degradation with bias, annealing, particle type and energy, bias conditions effects.

## B. Irradiation facilities

The three devices presented in previous section have been irradiated with protons, electrons, neutrons and gammas thanks to five different facilities. Two electron energies (0.5 and 1.5 MeV) were performed at GEODUR facility of ONERA (Toulouse, France) [27]. Van de Graaff accelerator provides mono-energetic beams and fluxes can be selected from 1 up to 100 nA/cm<sup>2</sup>.s ( $10^9 - 10^{12}$  e<sup>-</sup>/cm<sup>2</sup>.s) with non-uniformity lower than 10% within a beam diameter of 16 cm. Flux is measured thanks to Faraday cups. Global uncertainty of deposited fluence over samples is better than  $\pm 20\%$ .

Three higher electron energies (6, 12 and 20 MeV) were performed at RADEF facility (LINAC of University of Jyväskylä, Finland) [28]. This pulsed electron beam provides average dose rates ranging from 1 up to 10 Gy(water)/min. The beam non-uniformity and fluence measurement discrepancy is lower than  $\pm 5\%$  over 20 cm x 20 cm.

Some devices have also been irradiated with protons of 60, 100, and 170 MeV, as well as with atmospheric-like neutron spectrum of The Svedberg Laboratory (TSL, Uppsala, Sweden) facility [29]. Protons are produced with Gustaf Werner cyclotron providing beam intensities from 10  $\mu$ A down to few protons per second to PAULA user facility (Proton fAcility in Uppsala). Uncertainty on the deposited fluence due to dosimetry and beam non-uniformity was  $\pm 15\%$  for the largest beam diameter ( $\sim 20$  cm). Neutrons are delivered to Quasi-Monoenergetic Neutron (QMN) facility and ANITA facility (Atmospheric-like Neutrons from thIck Target). Spallation neutrons from ANITA spectrum are created with tungsten target. Neutron beams have continuous spectrum (Fig. 4) going from thermal energies up to  $\sim 180$  MeV. The neutron flux was in the order of few  $10^6$  cm<sup>-2</sup> s<sup>-1</sup> with a beam spot non-uniformity of  $\pm 5\%$  within  $\sim 20$  cm diameter. The part of thermal neutron flux represents less than 1% of the total integrated flux. Global uncertainty of deposited fluence was  $\pm 10\%$ . Based on NIEL of InGaAs material, the equivalent damage energy of the ANITA spectrum has been estimated to be around 2 MeV. This value is subjected to uncertainties from dosimetry (energy distribution and fluence level) and InGaAs NIEL estimation related to the choice of the nuclear database.

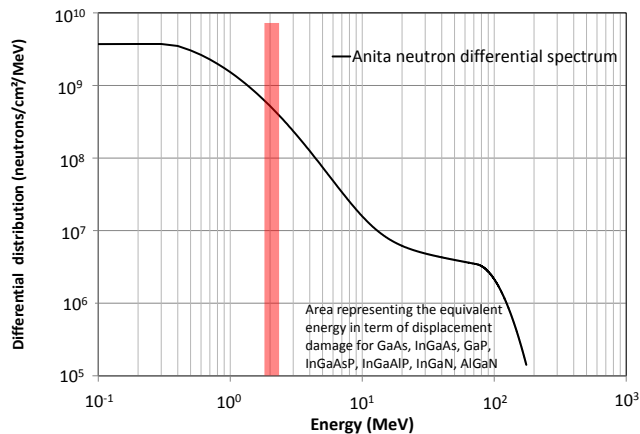


Fig. 4: Atmospheric-like neutrons spectrum provided by ANITA facility. Depending on tested material, the equivalent damage energy is found to be in the order of 2 MeV.

Some Total Ionizing Dose (TID) tests have also been performed with the CNA <sup>60</sup>Co facility (Centro Nacional de Aceleradores, Sevilla, Spain [42]), in order to check the sensitivity of devices to TID effect. Irradiation took more than four months to reach the final 5240 Gy level so that we did not perform the 24 h-annealing step recommended in ESA ESCC22900 specification, but devices were measured after two months annealing at room temperature. Irradiated devices have been placed inside lead/aluminum box. They have been covered by a sheet of PMMA (poly(methyl methacrylate)) in order to achieve conditions of equilibrium. Dosimetry was performed before irradiation using ionization chamber placed in the same conditions (i.e. inside a lead box). The accuracy of the dosimetry is within 5%. TABLE I and TABLE II summarize different irradiation steps.

## C. Test conditions

Photodiodes have been irradiated with two different bias conditions. Some devices have been shorted and others irradiated with a reverse bias. This is same bias conditions as those applied during dark current measurements: -10 V for the C30618 (Excelitas) and -5 V for both SNAKE (SOFRADIR) and FCIQ1000 (OSI). These biases correspond to large depletion regime dominated by generation current. Irradiations have been performed at ambient temperature ( $\sim 20^\circ\text{C}$ ). One device is irradiated per bias and energy. All devices are irradiated after removing the lid (no shielding between the beam and the photodiode). For each step of measurement, one non-irradiated sample was measured as a reference. Electrical measurements were performed with devices in complete dark condition inside a box with ambient temperature close to  $24^\circ\text{C}$ . Excelitas and OSI devices were inserted in aluminium block machined to ensure good thermal contact with devices. This block was equipped with a thermistor and TEC, stabilizing temperature to exactly  $24^\circ\text{C}$  and ensuring variation is lower than  $0.1^\circ\text{C}$  between measurements. SNAKE test vehicles were just put into the box, leading to larger uncertainty of the device temperature during measurements and much worse reproducibility. For the InGaAs gap, considering SRH carrier generation with activation energy close to mid-gap, an error of  $1^\circ\text{C}$  around  $24^\circ\text{C}$  corresponds to 5% error on dark current (close to 10% for  $2^\circ\text{C}$ ).

In this paper, dose values are given for InGaAs unless otherwise stated. As can be seen in TABLE I, applied fluences correspond to quite high levels of irradiation compared to most space radiation environments. The goal is to have a significant dark current increase that ensures some relevant measurements. But we avoid reaching and exceeding fluence of  $10^{12}$  particle/cm<sup>2</sup> in order to prevent any significant effect of carriers' removal. This phenomenon, which occurs for high fluence and subsequent high displacement damage doses, should not impact directly on dark current increase of photodiodes. For protons and high energy electrons, the fluences have been chosen in order to deposit same TID levels ( $\sim 320$  Gy). Hence, the final fluence and displacement damage dose are not identical from one irradiation to another. For low

energy electrons and gamma irradiations, the final dose is higher. But we provide intermediate steps at 300 Gy for electron and 450 Gy for gamma irradiations so that a comparison of degradation at same ionizing dose remains possible. In a global point of view, intermediate fluence steps with dark current measurements in between have been performed for neutron spectrum, 170 MeV protons, gamma rays, 0.5 MeV and 1.5 MeV electrons irradiations. These measurements were performed in order to check linearity of dark current increase as a function of fluence. The maximum applied displacement damage dose has been deposited with ANITA neutron spectrum ( $\sim 2.4 \cdot 10^{10}$  MeV/g). Annealing has been investigated thanks to measurements performed within one hour after the end of irradiation and two months later. The first step depends on access time to irradiated samples (venting and radio activation relaxation).

TABLE I: DDD LEVELS APPLIED ON PHOTODIODES FOR ALL IRRADIATIONS.

Particle type	Energy (MeV)	Fluence (p./cm <sup>2</sup> )	Fluence accuracy	TID level (Gy)	DDD level (MeV/g)
Neutrons (ANITA)	Spectrum	$3 \cdot 10^{11}$	10%	NA	$6.9 \cdot 10^{-8}$
		$3 \cdot 10^{12}$			$6.8 \cdot 10^{-9}$
		$10^{13}$			$2.4 \cdot 10^{10}$
Protons (PAULA)	60	$3 \cdot 10^{11}$	15%	320	$1.1 \cdot 10^{-9}$
	100	$4.3 \cdot 10^{11}$		320	$1.5 \cdot 10^{-9}$
	170	$3 \cdot 10^{11}$		152	$8.7 \cdot 10^{-8}$
Electrons (ONERA)	0.5	$10^{12}$	20%	200	$6.7 \cdot 10^{-6}$
		$1.5 \cdot 10^{12}$		300	$1.0 \cdot 10^{-7}$
		$2.5 \cdot 10^{12}$		500	$1.7 \cdot 10^{-7}$
	1.5	$5 \cdot 10^{11}$		100	$1.5 \cdot 10^{-7}$
		$10^{12}$		200	$2.9 \cdot 10^{-7}$
		$1.5 \cdot 10^{12}$		300	$4.3 \cdot 10^{-7}$
Electrons (RADEF)	6	$1.18 \cdot 10^{12}$	5%	325	$7.1 \cdot 10^{-7}$
	12	$9.22 \cdot 10^{11}$		333	$7.1 \cdot 10^{-7}$
	20	$7.16 \cdot 10^{11}$		339	$6.4 \cdot 10^{-7}$
<sup>60</sup> Co (CNA)	1.25	up to $\sim 4.5 \cdot 10^{14}$ (*)	5%	100	up to $\sim 4 \cdot 10^{17}$ (*)
				430	
				1050	
				2720	
				5240	

(\*) value estimated using GaAs NIEL instead of InGaAs one.

TABLE II: LIST OF IRRADIATIONS PER DEVICE TYPE.

Particle	E (MeV)	SNAKE		OSI		Excelitas	
		OFF	ON	OFF	ON	OFF	ON
n <sup>o</sup>	Spectrum	X	X	X	X	X	X
P+	60	X	X	X	X	X	X
	100			X	X	X	X
	170	X	X	X	X	X	X
e-	0.5	X		X	X	X	X
	1.5	X		X	X	X	X
	6	X		X		X	
	12	X					
	20	X		X		X	
<sup>60</sup> Co	1.25	X	X	X	X	X	X

#### IV. EXPERIMENTAL RESULTS

##### A. Dark current increase with fluence or ionizing dose

Shown in Fig. 5 are plots of OSI photodiodes responses for three different irradiation conditions: 170 MeV protons; neutrons from ANITA; Co-60 gammas. These three irradiations are selected because several fluences or dose levels are available. Initial dark current is between 0.1 and

0.5 nA over different samples. We can see that dark current increase is linear with fluence or TID. This trend is true for the three types of photodiodes. This linear dependence will allow extraction of damage factor as described in section V.

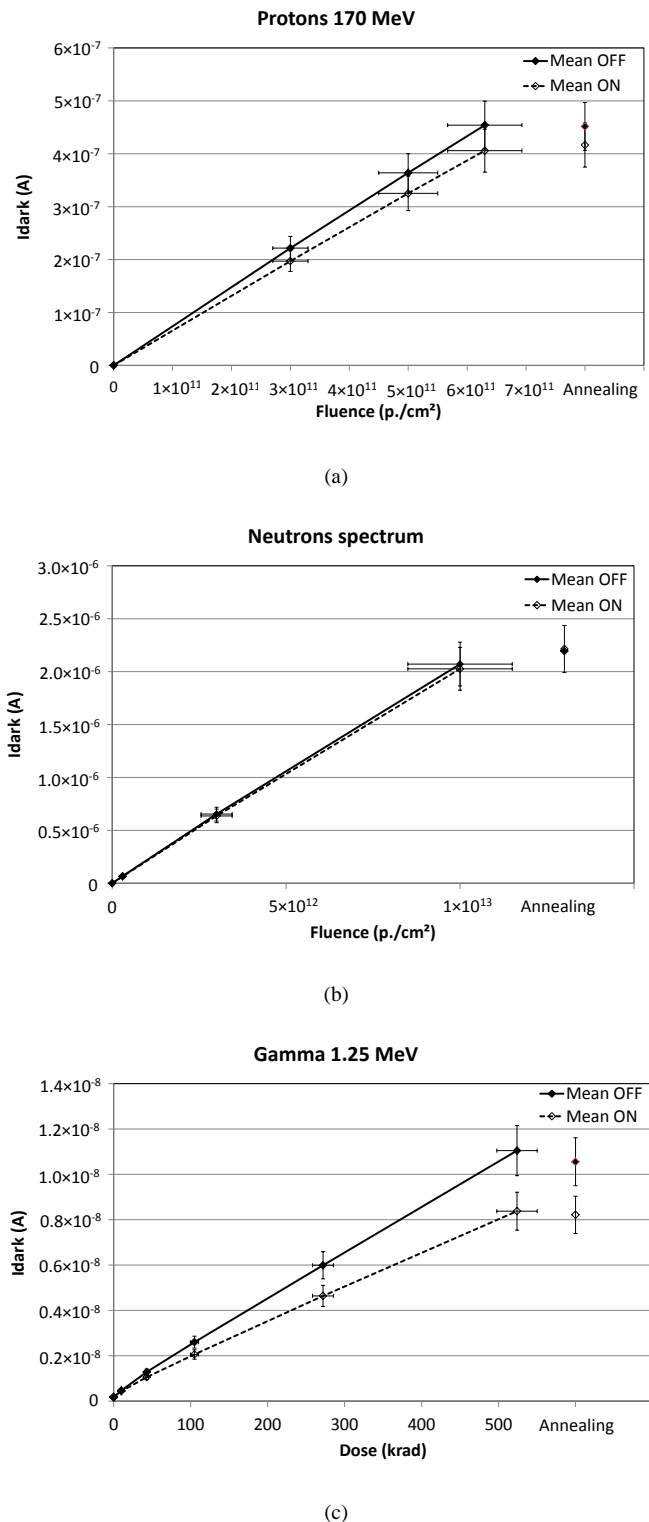


Fig. 5: Dark current of photodiodes FCIQ1000 (OSI) irradiated with (a) 170 MeV protons, (b) ANITA neutron spectrum and (c) gamma rays. Each figure details mean response over the four photodiodes of each device, irradiated biased or unbiased. The caption indicates bias condition during irradiation. Responses are linear as a function of DDD or TID.

Final TID level for gamma irradiations (5240 Gy) is much higher than TID reached after proton and electron irradiations (close to 320 Gy for protons and up to 500 Gy for electrons). Dark current increase is much lower for 500 Gy gamma than for other irradiations, except for 0.5 MeV electron where degradation is similar. The conclusion is that, for 1.5 MeV or higher electrons energies, protons and neutron irradiations, dark current degradation is dominated by displacement damage effects rather than TID effects.

The comparison between 0.5 MeV electrons and gamma irradiations will now be studied in more details for OSI and Excelitas devices (identical irradiated samples). TABLE III gives dark current increase per device after 0.5 MeV 500 Gy (final step) and gamma dose 430 Gy (closest step). TABLE III compares absolute values and variations for biased and unbiased devices. We can see that electrons and gamma rays induce similar dark current increases (difference of 30% before annealing and less than 10% after two month annealing). We must note that gamma irradiation can deposit displacement damage dose thanks to the interaction of secondary electrons with matter. This DDD has been evaluated using GaAs NIEL ( $9 \times 10^{-8}$  MeV.cm<sup>2</sup>/g [21] and TABLE I). Indeed, because NIEL of electrons in InGaAs and GaAs are close to each other, NIEL of gamma rays in these two materials should be close also. Both 500 Gy electron and 430 Gy gamma doses depict almost the same dark current increase while deposited DDD is five time larger for incident electrons ( $1.7 \times 10^{+07}$  Gy vs.  $3.3 \times 10^{+06}$  Gy). We conclude here that ionizing effects are dominant for gamma irradiation.

We should note that dose rates between gamma and electrons are different (500 to 1,000 times higher for electron) and that irradiation yields are also slightly different. Nevertheless, we conclude that TID effects are not negligible for 0.5 MeV electron irradiation, and may be the dominant contribution to dark current increase. This will be developed when comparing damage factors with NIEL in section V.

TABLE III: COMPARISON OF 430 GY GAMMA AND 500 GY 0.5 MEV ELECTRON IRRADIATIONS FOR OSI AND EXCELITAS PHOTODIODES DARK CURRENT.

Device	Gamma 430 Gy	0.5 MeV e- 500 Gy before annealing		0.5 MeV e- 500 Gy after annealing	
	$\Delta I$ (nA)	$\Delta I$ (nA)	Comp. $\gamma$	$\Delta I$ (nA)	Comp. $\gamma$
Excelitas OFF	1.58	2.28	30.7%	1.52	-4.1%
Excelitas ON	1.17	1.73	32.4%	1.27	7.8%
OSI OFF (*)	1.13	1.60	29.7%	1.06	-6.8%
OSI ON (*)	0.86	1.28	32.7%	0.96	9.8%

(\*) Mean value over the 4 samples of each device.

### B. Bias effect

Bias effect is only observable when both ON and OFF irradiations are made for a given particle type and energy. Thus, this analysis was performed for the three device types exposed to neutrons, protons, and gamma while only for OSI and Excelitas photodiodes with low energy electron irradiations (0.5 and 1.5 MeV, see TABLE II). Comparison is given in TABLE IV. For proton and neutron irradiations, difference is small and probably within the uncertainty of measurements and temperature control. Difference is more

obvious after gamma and low energy electron irradiations where it can reach up to 25%. Overall a lower degradation level is observed for biased devices during gamma irradiations.

TABLE IV: COMPARISON OF THE EFFECT OF BIAS CONDITIONS BEFORE ANNEALING.

Particle	E (MeV)	OSI(*)			Excelitas		
		$\Delta I$ (nA)		%	$\Delta I$ (nA)		%
		OFF	ON	OFF/ON	OFF	ON	OFF/ON
n <sup>o</sup>	Spectrum	2070	2030	2%	2460	2340	5%
P+	60	202	213	-6%	233	218	6%
	100	289	307	-6%	301	277	8%
	170	454	406	11%	476	419	12%
e-	0.5	1.6	1.3	20%	2.3	1.7	26%
	1.5	10.6	10	5%	15.5	12.5	18%
<sup>60</sup> Co	1.25	10.9	8.2	25%	14.6	10.7	27%

(\*) Mean value over the 4 samples of each device.

### C. Annealing effect

TABLE V: EFFECT OF TWO MONTHS ANNEALING AT ROOM TEMPERATURE.

Particle	E (MeV)	SNAKE		OSI		Excelitas	
		OFF	ON	OFF	ON	OFF	ON
n <sup>o</sup>	Spectrum	1.6%	0.6%	-6.0%	-9.3%	-3.1%	
P+	60	11.5 %	8.6%	-2.5%	-6.5%	0.9%	-4.1%
	100			1.9%	-1.5%	0%	-4.0%
	170	12.4 %	9.6%	0.5%	-2.6%	-1.5%	-4.6%
e-	0.5	18.3 %		27.4 %	17.4 %	33.4 %	26.7 %
	1.5	10.8 %		19.5 %	15.5 %	18.7 %	15.0 %
	6	6.2%		6.0%		5.5%	
	12	-1.1%					
	20	-3.9%		3.8%		2.9%	
<sup>60</sup> Co	1.25	-2.4%	0.3%	4.5%	1.9%	2.2%	0.6%

Recovery processes at room temperature have been shown to be negligible even two months after irradiation. This is also shown on Fig. 5. The detail of annealing percentage is given in TABLE V. Most of the time, annealing is close to 5% of the final dark current level just after irradiation for OSI and Excelitas devices. Two inconsistent annealing values are observed with low energy electrons. We suspect an error in thermal regulation during annealing measurements that were made at the same time on the same facility. Annealing of SNAKE samples is close to 10%, which is within the uncertainty of the device temperature. Results presented in the rest of the paper correspond to measurements two months after irradiation.

### D. Effect of the geometrical dimensions of photodiodes

In this section, we specifically investigate the relative degradation of SNAKE photodiodes with respect to active surface. Indeed, all photodiodes on test vehicles are made in the same technology, i.e. vertical dimensions of different photodiodes are the same. Main difference is linked to topology (circular or square shapes), surface and structure in the vicinity (for sub-arrays of pixels). So, if dark current increase is due to defects in semiconductor volume, it should be proportional to the surface of the different elements.

The comparison with OSI and Excelitas devices is not possible here because we do not have any information on device structure, except the active surface. As a consequence,

any differences in doping concentrations, vertical dimensions... will induce difference within active volume.

I(V) curves of all patterns from two test vehicles irradiated with 60 MeV protons (biased and unbiased) were measured several months after irradiation. The two test vehicles, labelled "Sample 1" and "Sample 2", come from two different InGaAs wafers. Fig. 6 shows the normalized dark current degradation: dark current after irradiation, much larger than dark current before irradiation (see Fig. 5), is divided by diode surface (area of the P-type region). The figure presents responses curves of both biased and unbiased test vehicles (during irradiation). All normalized curves follow the same trend within a factor of two. This confirms that increase of dark current is due to defects produced in the volume of photodiodes. Note that measurements of dark current presented in previous sections on SNAKE test vehicles were made at -5 V.

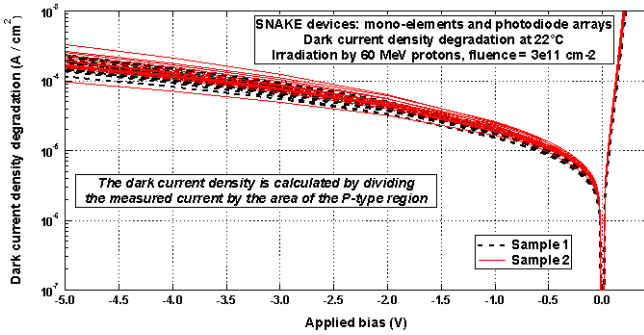


Fig. 6: I(V) curves of the different photodiode patterns. The current is normalized by the surface of diodes (i.e. the diffused P-type area). Measurements at 22°C.

## V. DARK CURRENT DAMAGE FACTOR

### A. Definition and evaluation

Damage factor is commonly used to compare degradation of devices for different particle types and energies due to displacement damage effects [6]-[8][16][18][19][23]. In our case, damage factor is calculated by dividing dark current increase by the applied fluence  $\Phi$ .

$$K_{I_{dark}} = \frac{I_{dark}(\Phi) - I_{dark}(0)}{\Phi} = \frac{\Delta I_{dark}(\Phi)}{\Phi} \quad (4)$$

with  $I_{dark}(\Phi)$  dark current at fluence  $\Phi$  and  $I_{dark}(0)$  initial dark current.

We should note that dark current increase is due to both ionizing ( $\Delta I_{dark,i}$ ) and non-ionizing ( $\Delta I_{dark,ni}$ ) effects:

$$\Delta I_{dark}(\Phi) = \Delta I_{dark,i}(\Phi) + \Delta I_{dark,ni}(\Phi) \quad (5)$$

As a consequence, the measured damage factor is the sum of ionizing and non-ionizing contributions:

$$K_{I_{dark}} = K_{I_{dark,i}} + K_{I_{dark,ni}} \quad (6)$$

with  $i$  and  $ni$  referring respectively to ionizing and non-ionizing effects.  $K_{I_{dark,i}}$  can be defined because dark current increase is proportional to TID for gamma irradiations, where ionizing effects are dominant.

We are interested here in the estimation of  $K_{I_{dark,ni}}$ , hence any ionizing contribution in the measurement of  $\Delta I_{dark}(\Phi)$  introduces an error in this estimation. Nevertheless, for all irradiations but 0.5 MeV electrons, dark current increase was dominated by displacement damage. In these cases,  $K_{I_{dark,i}} \ll K_{I_{dark,ni}}$  and  $K_{I_{dark}} \simeq K_{I_{dark,ni}}$ . For 0.5 MeV electrons,  $K_{I_{dark,i}}$  is not negligible anymore. Because it is difficult to determine ionizing contribution in dark current increase, we can only remark that  $K_{I_{dark,ni}} < K_{I_{dark}}$ . As a conclusion, the evaluation of  $K_{I_{dark,ni}}$  is not distorted by ionizing effects for all irradiations except the 0.5 MeV electron irradiation where it is overestimated.

Annealing after irradiation at room temperature in silicon device has been previously reported and synthesis can be found in [6]. It shows that annealing process decreases with time and is very slow after one month following irradiation. Even if few studies report significant annealing at room temperature in InGaAs materials, Yue et al. [44] shows that annealing occurs in III-V multi-junction solar cells at higher temperatures. In order to take into account possible annealing processes occurring shortly after irradiation and considering test conditions in [6] and [7], damage factors have been evaluated months after irradiation. Anyway, the previous section showed that annealing is small for our devices.

To evaluate damage factors, dark current increase has been divided by the surface of photodiodes. For OSI and Excelitas devices, optimal surface provided in datasheet have been used (350  $\mu\text{m}$  diameter,  $9.62 \cdot 10^{-4} \text{ cm}^2$  for Excelitas, 4 quadrants of one 1000  $\mu\text{m}$  diameter,  $7.85 \cdot 10^{-3} \text{ cm}^2$  each). For SNAKE test vehicles, surfaces of photodiodes have been provided by LYNRED. These values are smaller than the pitch of sub-arrays (this point will be discussed in paragraph V.B). Bulk damage are relative to the volume of the active region of devices. This volume was known for SNAKE devices, but not for commercial OSI and Excelitas photodiodes. Indeed, type and concentrations of dopants and layer thicknesses are probably different from one manufacturer to another. This prevented any absolute comparison of damage factors between the SNAKE and two other devices. Nevertheless, assuming a common depth of the active region for all photodiodes inside a SNAKE test vehicle, normalizing dark current increase with surface is relevant in order to compare the different topologies of SNAKE photodiodes.

This last section is devoted more specifically to the analysis of NIEL scaling approach validity. The Experimental damage factors for different particle types and energies are compared to their corresponding InGaAs NIEL. This comparison is performed relatively to one given particle type and energy ( $Part_0, E_0$ ). The damage factors of a given particle ( $Part, E$ ) are then normalized relatively to reference particle NIEL ( $Part_0, E_0$ ) according to following formula:

$$rel K_{I_{dark}}(Part., E) = \frac{K_{I_{dark}}(Part., E)}{K_{I_{dark}}(Part_0., E_0)} NIEL(Part_0., E_0) \quad (7)$$

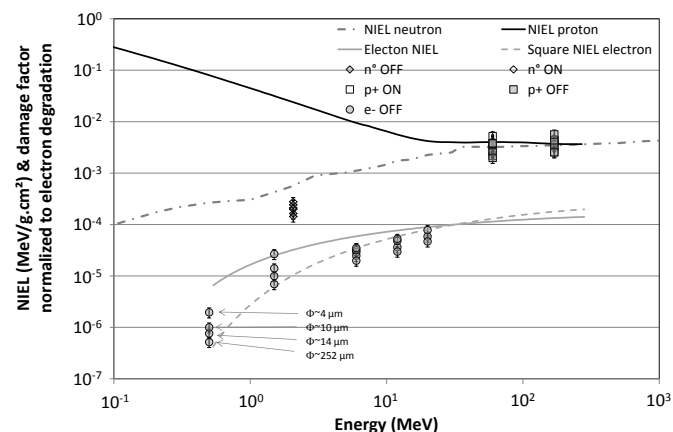
Where  $Part_0$  and  $E_0$  are the particle type and energy used as reference. The chosen reference particle is 2.07 MeV neutron because it is the equivalent energy of ANITA spectrum

( $\text{NIEL}_{n^0, 2.07 \text{ MeV}} = 5.71 \times 10^{-4} \text{ MeVcm}^2/\text{g}$ ). This choice has been made because no ionizing effects are expected for this kind of particle. More precisely,  $K_{I_{\text{dark}}}(n^0, 2.07 \text{ MeV})$  is the mean damage factor averaged for each device type (over different bias and topologies). Nevertheless, because equivalent fluence for neutron irradiations is subject to uncertainties (as presented in III.B), and in order to better correlate damage factors with both protons and electrons NIELs, the chosen normalisation factor was half the 2.07 MeV neutron NIEL ( $2.65 \times 10^{-4} \text{ MeVcm}^2/\text{g}$ ). This will be detailed in paragraph V.E.

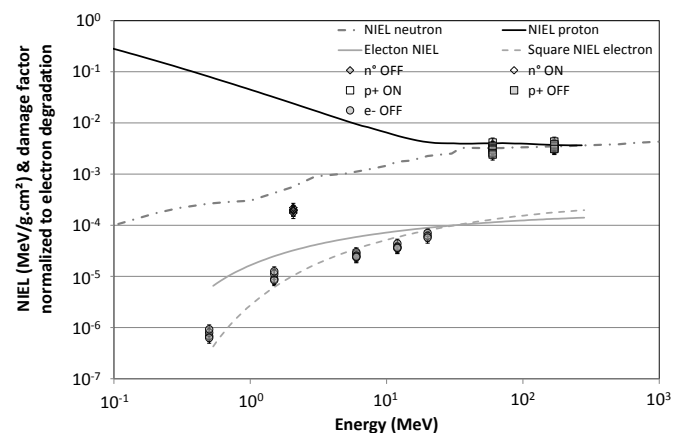
Assuming a maximum error of dosimetry of  $\pm 20\%$  and error in dark current measurement of  $\pm 10\%$ , we evaluate the error on damage factor as the quadratic sum of these two errors, close to  $\pm 22\%$  (error bars in Fig. 7 to Fig. 10).

### B. SNAKE relative damage factor

SNAKE devices present the advantage to propose different topologies. That leads to a scatter of dark current measurements. As already explained, dark current increase has been normalized to the surface of depleted region in order to achieve a proper comparison of data, regardless of photodiodes size. This point is highlighted in first part of this section.



(a)



(b)

Fig. 7: Comparison between dark current increase experimental damage factors for SNAKE test vehicles and NIEL of InGaAs. (a) using the diffusion surface evaluated by LYNRED and (b) correcting the diameter by  $2.5 \mu\text{m}$ .

Fig. 7 (a) presents the damage factor of all available data. As explained at the end of section V.A., experimental relative damage factors have been normalized to half of the 2.07 MeV neutron NIEL in order to better scale data with proton NIEL. Dispersion within data can be observed in Fig. 7 (a). Dispersion is quite significant for low energy electrons (factor of five). Unlike to OSI and Excelitas samples that have both large dimensions, some SNAKE samples have small diffusion diameters down to  $4 \mu\text{m}$ . Any error in the evaluation of diffusion diameter could lead to error in damage factor. Such a difference could occur if theoretical and effective diameters differ due for example to manufacturing processes.

In Fig. 7 (b), an offset of  $2.5 \mu\text{m}$  has been added to the diffusion diameter. This correction was suggested by the manufacturer. Indeed, this small value has great impact on small dimensions and the effect is clearly homogenization of the results. For the smallest photodiodes ( $4 \mu\text{m}$  diameter), an error of  $2.5 \mu\text{m}$  in diameter induces an error of 164% in the photodiode surface. This of course directly impacts on the comparison of damage factors from one topology to another. But for large photodiode dimensions (SNAKE, OSI and Excelitas), the diffusion area is close to optimal diameter of the topology and these two surfaces are almost the same. An error of  $3 \mu\text{m}$  in diameter induces an error smaller than 2% in photodiode surface. The offset of  $2.5 \mu\text{m}$  will be applied in the rest of the analysis for the SNAKE photodiodes.

### C. Proton relative damage factor for all device types

In Fig. 8, damage factors are compared with NIEL for protons. The same normalization factor as the one used in Fig. 7 is applied (i.e. half of the neutron NIEL for all devices). One can see that, for the three device types (OSI, Excelitas, SNAKE), damage factors follow total NIEL scaling. This is a difference compared to other publications that reported damage factor decreasing with proton energy above some tens of MeV, sometimes following the curve of NIEL Coulombian part.

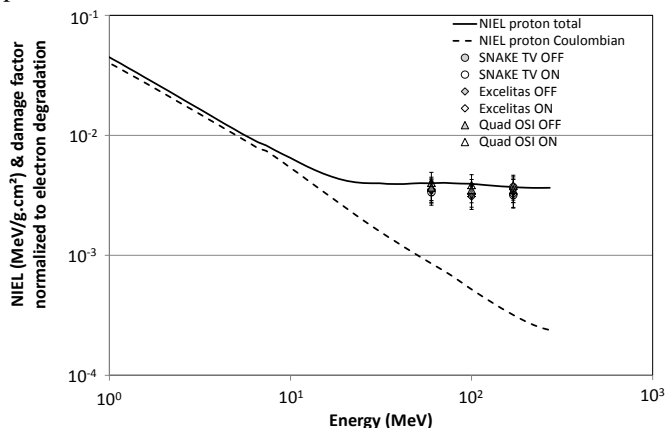


Fig. 8: Comparison between dark current increase experimental damage factors and NIEL of InGaAs for protons. SNAKE data correspond to mean value over different sizes of photodiodes.

#### D. Electron relative damage factor for all device types

In Fig. 9, the case of electrons is shown. We should note that, for such a comparison, we used different scale factors for OSI and Excelitas devices than for SNAKE. This can clearly be noticed in the following section where all damage factors are presented together. The consequence here is that one proposes a comparison of the damage factors variation with NIEL.

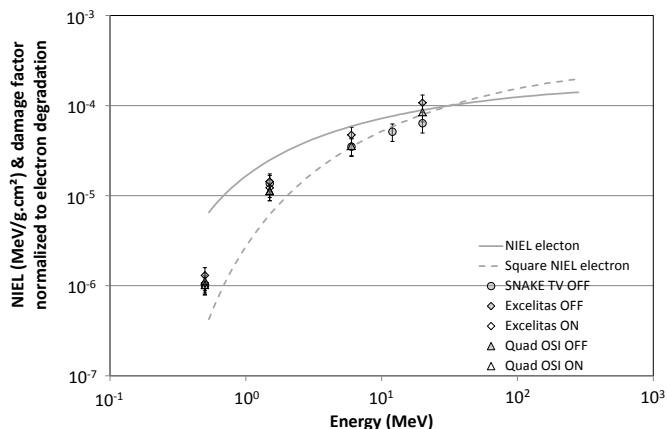


Fig. 9: Comparison between dark current increase experimental damage factors and NIEL of InGaAs for electrons. SNAKE data correspond to mean value over different sizes of photodiodes.

On the studied domain of energy, variation of the experimentally measured damage factors is greater than the one of electron NIEL. Indeed, the amplitude of damage factors variation between 0.5 MeV and 20 MeV is close to two decades, whereas variation of NIEL is close to ten. The measured damage factors behaviour is close to  $NIEL^2$ , which is also represented on the figure (dashed line). Such behaviour has been observed for silicon devices [6]. An interpretation was given in [45], related to worse calculation of low NIEL values.

#### E. Relative damage factors for all devices and particle types

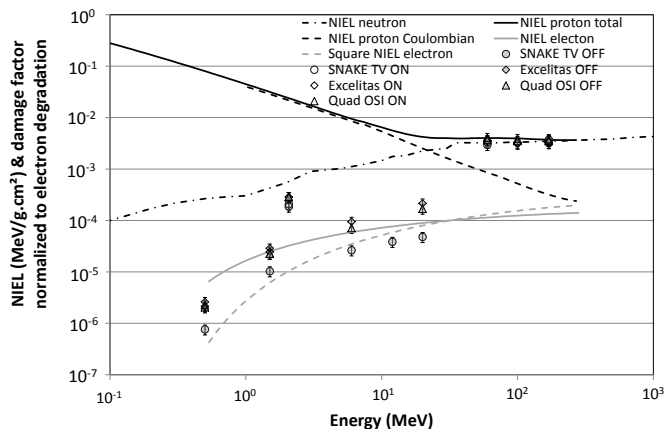


Fig. 10: Comparison between dark current increase experimental damage factors and NIEL of InGaAs for neutrons, protons and electrons. SNAKE data correspond to mean value over different sizes of photodiodes.

Finally, Fig. 10 compares damage factors all together. The normalization factor is the same for the three device types, i.e.

half of the 2.07 MeV InGaAs neutron NIEL. In this case, we see that 1) proton data fit with total NIEL, 2) neutron data are lower than neutron NIEL and 3) electron data are spread around electron NIEL. For the best fit, we could have chosen to normalize data with electron or neutron results. This would have shifted data up or down. But at this stage, it is difficult to conclude on the best way to normalize data. Anyway, because of the complex spectrum of neutron irradiations and the uncertainties in evaluation of equivalent energy and fluence, the difference between neutron NIEL and damage factors should not be considered as abnormal (factor two). But one must retain that the gap between proton and electron damage factors is not the same for OSI and Excelitas devices on one side, and SNAKE test vehicles on the other side. Fig. 10 shows that a factor close to four between all these data remains after normalization. One possible explanation could be due to different structures between three device types. But, as presented in first section, these structures are not available easily so that it is difficult at this stage to investigate deeper these discrepancies.

## VI. CONCLUSION

This work shows a large set of irradiation data i.e. dark current increase in different InGaAs photodiodes. The current increases linearly with fluence or TID. The degradation of different photodiode topologies is consistent with degradation in the volume of devices. Experimental damage factors are compared with NIEL for InGaAs material. Results show some differences in the ratio between proton and electron results from device type to the next. For high energy protons, the damage factors follow the total NIEL scaling. For electrons, NIEL overestimates low energy damage factors which seem to fit with a square function of NIEL.

## ACKNOWLEDGEMENTS

Results presented here were obtained in the framework of the EDA contract ROVER A-1341-RT-GP. Authors would like to thanks the European Defence Agency for supporting this study [46].

## REFERENCES

- [1] S. R. Messenger, E. A. Burke, G. P. Summers, M. A. Xapsos, R. J. Walters, E. M. Jackson, and B. D. Weaver, "Non ionizing energy loss (NIEL) for heavy ions," *IEEE Trans. Nucl. Sci.*, vol. 46, no. 6, pp. 1595–1602, Dec. 1999.
- [2] A. Akkerman, J. Barak, M. B. Chadwick, J. Levinson, M. Murat, and Y. Lifshitz, "Updated NIEL calculations for estimating the damage induced by particles and gamma-rays in Si and GaAs," *Rad. Phys. and Chem.*, vol. 62, pp. 301–310, 2001.
- [3] I. Jun, W. Kim, and R. Evans, "Electron nonionizing energy loss for device applications," *IEEE Trans. Nucl. Sci.*, vol. 56, no. 6, pp. 3229–3235, Dec. 2009.
- [4] C. Inguibert, and R. Gigante, "NEMO: A code to compute NIEL of protons, neutrons, electrons, and heavy ions," *IEEE Trans. Nucl. Sci.*, vol. 53, no. 4, pp. 1967–1972, Aug. 2006.
- [5] M. J. Boschini, C. Consolandi, M. Gervasi, S. Giani, D. Grandi, V. Ivanchenko, P. Nieminem, S. PenBotti, P. G. Rancoita, M. Tacconi, E. ESA, and A. G. Noordwijk, "Nuclear and non-ionizing energy-loss for Coulomb scattered particle from low energy up to relativistic regime in space radiation environment," in *Proc. the 12th ICATPP Conference on Astroparticle, Particle, Space Physics and Detectors for Physics Applications*, Como, Italy, pp. 9–23, Oct. 2010.

- [6] J. R. Srour, "Review of displacement damage effects in silicon devices," *IEEE Trans. Nucl. Sci.*, vol. 50, no. 3, pp. 653–670, Jun. 2003.
- [7] J. R. Srour, J. W. Palko " A framework for understanding displacement damage mechanisms in irradiated silicon devices," *IEEE Trans. Nucl. Sci.*, vol. NS-53, no.6, pp. 3610-3620 December 2006
- [8] G. P. Summers, E. A. Burke, C. Dale, E. A. Wolicki, P. W. Marshall, M. A. Gehlhausen, " Correlation of Particle-Induced Displacement Damage in Silicon, " *IEEE Trans. Nucl. Sci.*, vol. 34, no. 6, pp. 1133-1139, Dec. 1987.
- [9] S. R. Messenger G. P. Summers, E. A. Burke, R. J. Walters, and M. A. Xapsos, "Modeling solar cell degradation in space: A comparison of the NRL displacement damage dose and JPL equivalent fluence approaches," *Progress in Photovoltaics: Research and Applications*, vol. 9, pp. 103–121, 2001.
- [10] K. Thommen, "Recovery of low temperature electron irradiation-induced damage in n-type GaAs," *Radiation effects*, vol. 2, no. 3, pp. 201–210, 1970.
- [11] A. H. Kalma, R. A. Berger, C. J. Fischer, and B. A. Green, "Energy and temperature dependence of electron irradiation damage in GaAs," *IEEE Trans. Nucl. Sci.*, vol. 22, no. 6, pp. 2277–2282, Dec. 1975.
- [12] D. Pons, P. M. Mooney, and J. C. Bourgoin, "Energy-dependence of deep level introduction in electron-irradiated GaAs," *J. Applied Phys.*, vol. 51, no. 6, pp. 2038–2042, Apr. 1980.
- [13] M. Yamaguchi, C. Amano, "<sup>60</sup>Co  $\gamma$ -ray and electron irradiation damage of GaAs single crystals and solar cells," *J. Applied Phys.*, vol. 54, no. 9, pp. 5021–5029, Sep. 1983.
- [14] A. Meulenberg, C. M. Dozier, W. T. Anderson, S. D. Mittleman, M. H. Zuglich, and C. E. Caefar, "Dosimetry and total dose radiation testing of GaAs devices," *IEEE Trans. Nucl. Sci.*, vol. 34, no. 6, pp. 1745–1750, Dec. 1987.
- [15] M. A. Xapsos, G. P. Summers, C. C. Blatchley, C. W. Colerico, E. A. Burke, S. R. Messenger and P. Shapiro, "Co60 Gamma Ray and Electron Displacement Damage Studies of Semiconductors," *IEEE Trans. Nucl. Sci.*, vol. 41, no. 6, pp. 1945–1949, Dec. 1994.
- [16] G. P. Summers, E. A. Burke, P. Shapiro, S. Messenger, and R. J. Walters, "Damage correlations in semiconductors exposed to gamma, electron and proton radiations," *IEEE Trans. Nucl. Sci.*, vol. 40, no. 6, pp. 1372–1379, Dec. 1993.
- [17] G. P. Summers, E. A. Burke, and M. A. Xapsos, "displacement damage analogs to ionizing radiation effects," *Rad. Meas.*, vol. 24, no. 1, pp. 1–8, 1995.
- [18] J. H. Warner, S. R. Messenger, R. J. Walters, G. P. summers, J. R. Lorentzen, D. M. Wilt, M. A. Smith, "Correlation of electron radiation induced damage in GaAs solar cells," *IEEE Trans. Nucl. Sci.*, vol. 53, no. 4, pp. 1988–1994, Aug. 2006.
- [19] J. H. Warner, S. R. Messenger, R. J. Walters, G. P. Summers, " A comparison between p+n and n+p GaAs displacement damage coefficients following proton irradiation, " *33rd IEEE Photovoltaic Specialists Conference*, pp. 1-5, 2008.
- [20] P. Arnolda, C. Inguibert, T. Nuns, C. Boatella-Polo, "NIEL scaling: comparison with measured defect introduction rate in silicon," *IEEE Trans. Nucl. Sci.*, vol. 58, no. 3, pp. 756–763, Jun. 2011.
- [21] E. EL Allam, C. Inguibert, T. Nuns, A. Meulemberg, A. Jorio, I. Zorkani, "Gamma and Electron NIEL Dependence of Irradiated GaAs," *IEEE Trans. Nucl. Sci.*, vol. 64, no. 3, pp. 991–998, Mar. 2017.
- [22] G. P. Summers, E. A. Burke, M. A. Xapsos, C. Dale, P. W. Marshall, E. L. Petersen, " Displacement damage in GaAs structures, " *IEEE Trans. Nucl. Sci.*, vol. 35, no. 6, pp. 1221-1226, Dec. 1988.
- [23] S. R. Messenger, R. J. Walters, E. Burke, G. P. Summers, and M. A. Xapsos, "NIEL and damage correlations for high-energy protons in gallium arsenide devices," *IEEE Trans. Nucl. Sci.*, vol. 48, no. 6, pp. 2121–2126, Dec. 2001.
- [24] A. Barry, A. Houdayer, P. Hinrichsen, W. Letourneau, and J. Vincent, "Energy dependence of lifetime damage constants in GaAs LEDs for 1–500 MeV protons," *IEEE Trans. Nucl. Sci.*, vol. 42, pp. 2104–2107, Dec. 1995
- [25] A. M. Ougouag, J.G. Williams, M. B. Danjaji, J. L. Yang, J. L. Meason, "Differential displacement kerma cross sections for neutron interactions in Si and GaAs," *IEEE Trans. Nucl. Sci.*, vol. 37, no. 6, Part II, pp. 2219–2228, Dec. 1990.
- [26] O. Gilard, L. S. How, A. Delbergue, C. Inguibert, T. Nuns, J. Barbero, J. Moreno, L. Bouet, S. Mariojouis, M. Boutillier, "Damage Factor for Radiation-Induced Dark Current in InGaAs Photodiodes," *IEEE Trans. Nucl. Sci.*, vol. 65, no. 3, Part II, pp. 884–895, Mar. 2018.
- [27] GEODUR: Chambre d'irradiation électrons multi applications (matériaux, composants, charge interne des isolants. [Online]. Available: <http://www.onera.fr/fr/desp/geodur> Accessed July 27, 2017.
- [28] RADEF: Jyväskylä Yliopisto, University of Jyväskylä. [Online]. Available: <https://www.jyu.fi/fysiikka/en/research/accelerator/radef>. Accessed July 27, 2017.
- [29] The ANITA neutron beam facility [Online]. Available: [http://www.tsl.uu.se/irradiation-facilities-tsl/ANITA\\_neutron\\_beam\\_facility/](http://www.tsl.uu.se/irradiation-facilities-tsl/ANITA_neutron_beam_facility/) Accessed July 27, 2017.
- [30] M. Robinson, "The dependence of radiation effects on the primary recoil energy, " in Proc. Int. Conf. Radiation-Induced Voids in Metal, Albany NY, pp. 397-429, 1972.
- [31] A. Jr. McKinley and A. Fesbach, "The Coulomb Scattering of Relativistic Electrons by Nuclei, " *Phys. Rev*, vol. 74, pp. 1759-1763, 1948
- [32] GEANT4 a simulation toolkit, [Online]. Available: <https://geant4.web.cern.ch/> Accessed January, 7, 2020.
- [33] D.H.Wright, M.H.Kelse "The Geant4 Bertini Cascade, " *Nuc. Instr. & Meth. In Phys. Res. A*, Vol. 804, no. 21, pp. 175-188, 2015.
- [34] NJOY, [Online] Available: <http://www.njoy21.io/> Accessed January, 7, 2020.
- [35] M. G. Catanesi, et al (HARP collaboration). "Large-angle production of charged pions with 3–12.9 GeV/c incident protons on nuclear targets, " *Phys. Rev. C*, vol. 77, pp. 055207-1-055207-49, 2008.
- [36] Screened Relativistic (SR) Nuclear Stopping Power Calculator, [Online] Available <http://www.sr-niel.org/> Accessed January, 7, 2020.
- [37] ASTM E722-14, Standard Practice for Characterizing Neutron Fluence Spectra in Terms of an Equivalent Monoenergetic Neutron Fluence for Radiation-Hardness Testing of Electronics, ASTM International, West Conshohocken, PA, 2014.
- [38] OMERE: Outil de Modélisation de l'Environnement Radiatif Externe, version 4.2. [Online]. Available: <http://www.trad.fr/OMERE-14.html> Accessed July 27, 2017.
- [39] LYNRED: Lynred [Online]. Available: <https://www.lynred.com> Accessed September 10, 2019; notice that Sofradir became Lynred in 2019.
- [40] EXCELITAS: Excelitas technologies. [Online]. Available: <http://www.excelitas.com/Pages/Index.aspx> Accessed July 27, 2017.
- [41] OSI: OSI Optoelectronics. [Online]. Available: <http://www.osioptoelectronics.com/standard-products/silicon-photodiodes.aspx> Accessed July 27, 2017.
- [42] CAN: Centro Nacional de Aceleradores [Online]. Available: <http://www.centro.us.es/cna/index.php/en/facilities/co-60-irradiator> Accessed April 10, 2019.
- [43] T. P. Ma and P. V Dressendorfer, "Ionizing radiation effects in MOS devices and circuits," Wiley Interscience publication, 1989.
- [44] L. Yue, Y. Wu, Q. Fu, and Y. Zhang, 'Study on annealing effects of irradiated Ga0.5In0.5P/GaAs/Ge solar cell by 170 keV proton', in *2014 10th International Conference on Reliability, Maintainability and Safety (ICRMS)*, Guangzhou, China, pp. 82–85, 2014.
- [45] C. Inguibert, P. Arnolda, T. Nuns, G. Rolland, "Effective NIEL in Silicon: Calculation using molecular dynamic results," *IEEE Trans. Nucl. Sci.*, vol. 57, no. 4, pp. 1915–1923, 2010.
- [46] The European Defence Agency [Online]. Available: <https://www.eda.europa.eu/> Accessed July 27, 2019.
- [47] R. A. Weller, M. H. Mendenhall, and D. M. Fleetwood, "A screened Coulomb scattering module for displacement damage computations in Geant4," *IEEE Trans. Nucl. Sci.*, vol. 51, no. 6, pp. 3669-3678, Dec. 2004.